Linking granulation performance with residence time and granulation liquid distributions in twin-screw granulation: an experimental investigation

Ashish Kumar[a,b], Maija Alakarjula[c], Valérie Vanhoorne[d], Maunu Toiviainen[e], Fien De Leersnyder[b], Jurgen Vercruysse[d], Mikko Juuti[e], Jarkko Ketolainen[c], Chris Vervaet[d], Jean Paul Remon[d], Krist V. Gernaey[f], Thomas De Beer[b,1], Ingmar Nopens[a,*]

[a] *BIOMATH, Dept. of Mathematical Modelling, Statistics and Bioinformatics, Faculty of Bioscience Engineering, Ghent University, Coupure Links 653, B-9000 Gent, Belgium*
[b] *Laboratory of Pharmaceutical Process Analytical Technology, Dept. of Pharmaceutical Analysis, Faculty of Pharmaceutical Sciences, Ghent University, Harelbekestraat 72, B-9000 Ghent, Belgium*
[c] *School of Pharmacy, University of Eastern Finland, Kuopio, Finland*
[d] *Laboratory of Pharmaceutical Technology, Dept. of Pharmaceutics, Faculty of Pharmaceutical Sciences, Ghent University, Harelbekestraat 72, B-9000 Ghent, Belgium*
[e] *Optical Measurement Technologies, VTT Technical Research Centre, Kuopio, Finland*
[f] *CAPEC-PROCESS Research Center, Department of Chemical and Biochemical Engineering, Technical University of Denmark, DK-2800 Kongens Lyngby, Denmark*

*Email address: ingmar.nopens@ugent.be, Tel.: +32 (0)9 264 61 96; fax: +32 (0)9 264 62 20
Email addresses: ashish.kumar@ugent.be (Ashish Kumar), maijaa@student.uef.fi (Maija Alakarjula), valerie.vanhoorne@ugent.be (Valérie Vanhoorne), maunu.toiviainen@vtt.fi (Maunu Toiviainen), fien.deleersnyder@ugent.be (Fien De Leersnyder), jurgen.vercruysse@ugent.be (Jurgen Vercruysse), mikko.juuti@vtt.fi (Mikko Juuti), jarkko.ketolainen@uef.fi (Jarkko Ketolainen), chris.vervaet@ugent.be (Chris Vervaet), jeanpaul.remon@UGent.be (Jean Paul Remon), kvg@kt.dtu.dk (Krist V. Gernaey), thomas.debeer@ugent.be (Thomas De Beer)
URL: www.biomath.ugent.be (Ingmar Nopens)
[1] Shared last authorship

Preprint submitted to European Journal of Pharmaceutical Sciences *November 25, 2015*

Abstract

Twin-screw granulation is a promising wet granulation technique for the continuous manufacturing of pharmaceutical solid dosage forms. A twin screw granulator displays a short residence time. Thus, the solid-liquid mixing must be achieved quickly by appropriate arrangement of transport and kneading elements in the granulator screw allowing the production of granules with a size distribution appropriate for tableting. The distribution of residence time and granulation liquid is governed by the field conditions (such as location and length of mixing zones) in the twin-screw granulator, thus contain interesting information on granulation time, mixing and resulting sub-processes such as wetting, aggregation and breakage. In this study, the impact of process (feed rate, screw speed and liquid-to-solid ratio) and equipment parameters (number of kneading discs and stagger angle) on the residence time (distribution), the granulation liquid-powder mixing and the resulting granule size distributions during twin-screw granulation were investigated. Residence time and axial mixing data was extracted from tracer maps and the solid-liquid mixing was quantified from moisture maps, obtained by monitoring the granules at the granulator outlet using near infra-red chemical imaging (NIR-CI). The granule size distribution was measured using the sieving method. An increasing screw speed dominantly reduced the mean residence time. Interaction of material throughput with the screw speed and with the number of kneading discs led to most variation in the studied responses including residence time and mixing capacity. At a high screw speed, granulation yield improved due to high axial mixing. However, increasing material throughput quickly lowers the yield due to insufficient mixing of liquid and powder. Moreover, increasing liquid-to-solid ratio resulted in more oversized granules, and the fraction of oversized granules further increased at higher throughput. Although an increasing number of kneading discs was found to be critical for achieving a uniform distribution of the granulation liquid, the granulation performance was hampered due to insufficient solid-liquid mixing capacity of the current kneading discs which is essential for

wet granulation. Thus, a balance between material throughput and screw speed should be strived for in order to achieve a specific granulation time and solid-liquid mixing for high granulation yield. Additionally, more efforts are needed both in modification of the screw configuration as well as the geometry of the mixing elements to improve the mixing capacity of the twin-screw granulator. The results from the current experimental study improved the understanding regarding the interplay between granulation time and the axial and solid-liquid mixing responsible for the granulation performance in twin-screw wet granulation.

Keywords: residence time distribution, axial mixing, NIR chemical imaging, solid-liquid mixing

1. Introduction

Efforts towards switching from batch to continuous processing with 24/7 production capacity form one of the major considerations in the pharmaceutical industry for improving the operational efficiency, including enhancing quality assurance (Poechlauer et al., 2012). However, a transformation to completely continuous processing requires all the unit operations to be performed in a continuous mode with inter-compatibility, both in terms of capacity and processing time. In this context, twin-screw granulation has emerged as a promising technology for continuous wet granulation in continuous solid dosage manufacturing. A manufacturing line with continuous twin-screw granulator (TSG) followed by (semi-)continuous drying, milling and tableting units is conceptualised for a continuous 'from powder to tablet' manufacturing system. Several studies have shown that the mean residence time $\bar{t}$ in a TSG (which is generally between 2 and 40 seconds) is much shorter compared to the granulation time available in a typical batch granulator, which is in the order of minutes (Kumar et al., 2013). Thus, the solid-liquid mixing in the TSG must be achieved in a short period by appropriate arrangement of transport and kneading elements in the granulator barrel allowing

the production of granules with a granule size distribution (GSD) suitable for downstream operations (drying, tableting, etc.). Therefore, it is interesting to investigate how different process and equipment settings lead to changes in the residence time distribution (RTD), axial and solid-liquid mixing which consequently lead to a certain granulation yield. This is particularly important as it could be concluded from an earlier study that a residence time increase beyond a certain threshold is the result of a change in flow regime inside the TSG, transitioning from mixed flow to plug flow (Kumar et al., 2014). As the plug flow regime cannot be desired for mixing which is ultimately required for granulation, a detailed study investigating the link between mixing and transport characteristics in the TSG and the granulation performance is required.

Experimental investigation of twin-screw granulation RTD and its impact on granulation performance has already been of interest for several other research groups. Dhenge et al. (2010) measured the RTD using the sampling cup method under different processing conditions and showed that process parameters such as screw speed and liquid-to-solid ratio (L/S) have vital influence on the residence time. The same RTD measurement approach was applied by El Hagrasy et al. (2013) to estimate the effect of changes in formulation properties such as raw material composition as well as granulation liquid properties such as viscosity on the granule properties. However, $\bar{t}$ for a typical screw design is between 2-40 s which is in the order of the sampling time in the sampling cup method, making this method unsuitable for TSG studies (Li et al., 2014). In a remarkable attempt, Lee et al. (2012) obtained the RTD for TSG using positron emission particle tracking (PEPT) to study the axial mixing of the processed material inside the TSG barrel, which is essential information for the optimisation of the obtained granule properties. Although PEPT is very powerful technique, this method based on the single-particle tracking also suffers from major challenges as discussed by Kumar et al. (2014, 2015). Recently, Li et al. (2014) used a visual

technique based on digital video recording to measure RTD as a function of feed rate during twin-screw granulation. Results from that study indicated a significant increase in $\bar{t}$ and a narrowing of RTD at higher feed rate. The study questioned the role of the kneading block as mixing zone which is atypical since RTD can only be used to quantify axial mixing. Mixing of solid-liquid is typically driven by a combination of both axial and transverse mixing inside the TSG. Thus, this cannot be investigated solely from an RTD study. However, only a small number of investigations have attempted to quantitatively describe the influence of process parameters on solid-liquid mixing performance (Vercruysse et al., 2013). This is mainly because of the lack of suitable techniques allowing detailed local flow characterisation in systems such as the TSG, especially due to their opacity. Vercruysse et al. (2013) applied an image data collection method based on near infrared (NIR) chemical imaging to evaluate the influence of the screw configuration, liquid addition method and rate, and the barrel filling degree on the moisture homogeneity during twin-screw granulation. Applying the same measurement approach, a tracer (theophylline anhydrate) was injected in the granulator and monitored to investigate the RTD of the tracer inside the barrel as a function of screw speed, material throughput and number as well as stagger angle of the kneading discs in the screw configuration of the TSG. Model-based analysis of these experimental data was also performed to further investigate the mixing and flow behaviour inside the TSG (Kumar et al., 2015). However, a relation between granulation time (measured as the mean residence time) and the mixing quality (measured as the axial mixing and the solid-liquid mixing), all responsible for the shape of the granule size distribution, is still not established.

In the present study, NIR chemical imaging was used as analytical technique to simultaneously and qualitatively and quantitatively characterise the flow and axial mixing of tracer material as well as the mixing of the two phases, i.e. solid formulation material and granulation liquid, as function of process (screw speed, material throughput and liquid-to-solid

ratio) and equipment (number and stagger angle of kneading discs in the screw configuration) parameters of the twin-screw granulation. Since residence time and its distribution, as well as solid-liquid mixing dictate the final granulation yield, the resulting GSD was also measured to understand the overall influence of different flow and mixing conditions.

2. Materials and methods

2.1. Pharmaceutical formulation

α-Lactose monohydrate (Pharmatose 200M, Caldic, Hemiksem, Belgium) was used as model excipient. Distilled water was added as granulation liquid. To evaluate the residence time of the material inside the barrel, theophylline anhydrate (Farma-Química Sur, Malaga, Spain) was used as tracer component.

2.2. Continuous twin screw granulation

Granulation experiments were performed using a 25 mm diameter co-rotating TSG, which is the granulation module of the ConsiGma-25 unit (GEA Pharma Systems, Collette™, Wommelgem, Belgium). The granulator screw has a length-to-diameter ratio of 20:1 (Fig. 1). The TSG barrel consists of a feed segment, where the powder enters the barrel and is transported through the conveying zone to the work segment, where the granulation liquid is added to the powder which is further intensively mixed by a combination of kneading discs and transport elements. The screw configuration is composed of kneading zones consisting of maximum 6 kneading discs in each zone (Length = $^{Diameter}/_{4}$ for each kneading element) at an angle of 30° and 60° (Fig. 1). Both kneading zones are separated by a conveying element (Length = 1.5 Diameter). When more than six kneading discs are used, an extra conveying element (Length = 1.5 Diameter) is implemented between the two mixing zones. Two narrow kneading discs (Length = $^{Diameter}/_{6}$) were placed at the end of each screw in order to reduce the amount of oversized agglomerates, as reported by Van Melkebeke

et al. (2008). The barrel jacket is preheated to 25°C. During processing, pure α-lactose monohydrate is gravimetrically fed into the granulator by using a twin-screw feeder (KT20, K-Tron Soder, Niederlenz, Switzerland). Distilled water as granulation liquid is pumped into the screw chamber by using a peristaltic pump (Watson Marlow, Cornwall, UK) and silicon tubings connected to the nozzles of diameter 1.6 mm. The granulation liquid is added before the first kneading element by dripping through two liquid feed nozzles, each nozzle located on top of each screw in the barrel (Kumar et al., 2014). A pulse of anhydrous theophylline (2% (w/w) of the material throughput) used as tracer is manually added into the powder inlet port of the granulator. The TSG has an inbuilt torque gauge and the steady state criteria are decided on the equilibration of the measured torque of the granulator. The torque values obtained after equilibration of the process are averaged to give the overall torque during each run.

[Figure 1 about here.]

2.3. Description of NIR chemical imaging setup

Wet granules from the granulator output fall on a conveyor belt (Mini, ENP, Hjälteby, Sweden) which is moving at a speed of 3.12 cm/s. Spectral images of the wet granules are collected using a line-scanning (pushbroom) hyperspectral camera (SWIR, Specim Ltd., Oulu, Finland). The camera sees a row of 320 spatial pixels at a time, and disperses the incoming light from each pixel in the spectral range 970-2500 nm onto one column of the 320×256-pixel mercury-cadmium-telluride (MCT) detector (14-bit readout, cooled to -70°C with a 4-stage Peltier system). The camera-to-belt distance is set such that the imaged line had a length of 10 cm on the conveyor belt, and the speed of the conveyor belt is adjusted to achieve a spatial resolution of 312×312 μm^2 per pixel at the maximum frame rate permitted by the camera (100 frames per second). The conveyor belt and the sample material on it were illuminated with two rows of three 75-W halogen lamps (Specim Ltd., Oulu, Finland)

at a distance of 35 cm, and the measurement is conducted in diffuse reflectance mode in the 45°-0°-45° geometry (For details see (Kumar et al., 2014)). Each collected spectral image consists of 2500 frames (25 seconds measurement, 2500×320 spatial pixels, 256-element spectrum at each spatial pixel) which corresponds to an area of 10×64 cm^2 on the conveyor belt. At a material throughput of 10-25 kg/h the dry mass of material in one spectral image is approximately 69-173 g.

Extraction of relevant information from spectral data

The analysis of the hyperspectral images from the RTD and solid-liquid measurements is performed in two steps. In a first step, spatial pixels corresponding to the plastic conveyor belt were eliminated from the data set via partial least squares discriminant analysis (PLS-DA) classification (Kumar et al., 2014). In the second step, the NIR spectra in the remaining pixels corresponding to the granules were subjected to semi-quantitative analysis of theophylline content and moisture content. In both cases, the spectral range was narrowed to 1100-2200 nm and the spectra were subjected to the standard normal variate (SNV) pretreatment to eliminate the additive baseline offset variations and multiplicative scaling effects in the spectra which may be caused by experimental conditions such as shadowed regions near large granules and possible differences in granule density. Subsequently, a measure for the theophylline level was used to quantify the RTD using the spectral matched filter (SMF) method which provides a highly selective response for the target analyte. A measure for the moisture level was obtained for studying solid-liquid mixing using the band ratio method (Fig. 2) (Vercruysse et al., 2013). The NIR chemical imaging measurement setup and extraction of relevant information from chemical images was discussed in more detail by Vercruysse et al. (2013) and is schematically shown by Kumar et al. (2014).

[Figure 2 about here.]

2.4. Experimental design

2.4.1. Experimental procedure

A full factorial experimental design was performed to evaluate the influence of screw speed (500-900 rpm), material throughput (10-25 kg/h), L/S (6-8%), number (4, 6, 12) and stagger angle (30°, 60°) of the kneading discs in the screw configuration on the RTD and axial mixing of the material. Three center point experiments were performed as well, resulting in 48 + 3 = 51 experiments.

At the outlet of the granulator, the near infrared chemical imaging (NIR-CI) system was used to measure solid-liquid mixing and the theophylline dynamics. A 25 s chemical imaging measurement without tracer injection for each design experiment (run) was used to measure the spatial distribution of the granulation liquid which was calculated using the band ratio method explained in section 2.3. For the residence time measurements, anhydrous theophylline (2% (w/w) of the material throughput per minute, corresponding to 3.33, 5.83 and 8.33 g for throughputs of 10, 17.5 and 25 kg/h respectively) was spiked. Since it took 5 s for the conveyor belt to move from below the granulator output to the location of the spectral image collection, the chemical imaging measurements were started 5 s after injecting the tracer (theophylline) for each experiment. Thus, the first frame of the spectral image corresponded to the instant of theophylline addition. The spatial distribution of theophylline during the 25 s measurement was calculated with the SMF method as explained in section 2.3.

The intensity of the pixels in the obtained chemical map was thus proportional to the true moisture and theophylline levels. Hence, the moisture distribution and the RTD for each run was determined via inspecting the temporally scanned direction of the spectral image.

2.4.2. Estimation of RTD and axial mixing efficiency

Conventionally, a RTD is obtained by injecting a pulse of tracer into the system at the inlet, and the residence time function, $e(t)$, is calculated as

$$e(t) = \frac{c(t)}{\int_0^\infty c(t)dt} \tag{1}$$

where $c(t)dt$ is the concentration of the tracer at the outlet between t and $t + \Delta t$. In this study, the exit age distribution of the tracer molecule (theophylline) was derived from the tracer concentration c_i (as estimated using the SMF method) between t and $t + \delta t$ in the temporal profile of the discrete tracer map (top of Fig 2) calculated as

$$e(t) = \frac{c_i}{\sum_{i=1}^{t} c_i \Delta t} \tag{2}$$

This tracer map was transformed into the exit age distribution curve, i.e. the RTD based on the mean tracer concentration, $e(t)$ between t and $t + dt$ (RTD plot in Fig 2), which was then used to calculate the mean residence time $\bar{t}$ as the ratio of the first and the zeroth moment using the following equation

$$\bar{t} = \frac{\int_0^\infty t.e(t)dt}{\int_0^\infty e(t)dt} \tag{3}$$

The RTD shape, was normalised as $e(\theta) = \bar{t}.e(t)$, where dimensionless time $\theta = {}^{t}/_{\bar{t}}$ is introduced. The degree of axial mixing in the granulator can be quantified by calculating the dimensionless Péclet number Pe which represents the ratio of the rate of axial transport by convection and axial transport by diffusion or dispersion. By treating the boundary condition of the granulator as a closed system with no dispersion or radial variation in concentration either upstream or downstream, the following equation can be derived (Fogler,

2006)

$$\frac{\sigma_{\bar{t}}^2}{\bar{t}^2} \approx \frac{2\mathrm{Pe} - 2 + 2 \cdot e^{-\mathrm{Pe}}}{\mathrm{Pe}^2} \tag{4}$$

where, the $\sigma_{\bar{t}}^2$, which measures the width of the RTD, is calculated as:

$$\sigma_{\bar{t}}^2 = \frac{\int_0^\infty (t - \bar{t})^2 . e(t) dt}{\int_0^\infty e(t) dt} \tag{5}$$

and the $\sigma_{\bar{t}}^2/\bar{t}^2$ in eq. 4 represents the normalised variance σ_θ^2, which is the normalised second central moment of the RTD curve. When σ_θ^2 approaches zero, Pe tends to infinity indicating that the extent of axial mixing is low. Thus, when the Pe turns out to be large, the granulator characteristics approach those of a plug-flow reactor (PFR). This regime is not favourable in continuous processing as the existence of plug flow indicates poor axial mixing in the granulator which is not desirable as discussed by Kumar et al. (2014). The study showed that conditions leading to a greater extent of plug flow ultimately result in a complete disruption due to jamming of the TSG.

2.4.3. Estimation of moisture distribution

A large amount of chemical imaging data were collected resulting in spatio-temporal moisture maps of wet granules for each experimental run (Fig. 2). The liquid-solid mixing can be seen as a process in which a complex liquid exchange network between particles of the processed material is generated. The pixel intensity values in the moisture maps are indicative of this liquid exchange level or distribution. The statistical phenomena on uncertainty of the pixel intensity at a randomly selected point on the moisture map can be quantified as Shannon entropy (Guida et al., 2010) given as,

$$H(X) = \sum_{j=1}^{n} P(X_j) \log_{256}(1/P(X_j)) = -\sum_{j=1}^{n} P(X_j) \log_{256} P(X_j) \tag{6}$$

where X is the value of the pixel index j and n is total number of pixels in the moisture map. The Shannon entropy, which is used in Information Theory, thus appears to be a useful parameter for describing the mixing efficiency in a system (Guida et al., 2010). Since the moisture maps were not calibrated for quantitative moisture content determination, entropy was selected to evaluate the liquid distribution. Entropy only envisages the distribution itself and not the values that pixel intensity may take. In this study, the logarithm to the base 256 was applied, as the 8-bit moisture map allows displaying the moisture distribution using 256 different intensities. Since a progression in mixing causes an increase in uncertainty of pixel intensity transitions in the moisture map, a mixing index (MI) based on such an uncertainty was defined as:

$$\mathrm{MI} = -\frac{1}{\log_{256}(n)} \sum_{j=1}^{n} P(X_j) \log_{256} P(X_j) \tag{7}$$

The mixing index (MI) value lies between 0 and 1 indicating "no mixing" and "perfect mixing" of the granulation liquid, respectively.

Since the MI is derived from the bulk solid-liquid mixing outcome, hereby completely avoiding the dynamics of the mixing process which lead to variations in mean moisture content in the granules produced at different times, an additional method based on calculation of frequency and amplitude of variations in the mean profile of the moisture content was used to quantify the perturbations in the solid-liquid mixing (Fig. 3). A lowpass filter was applied on the fast Fourier transform (FFT) of the mean moisture profile to remove noise and only extract the main frequency and its amplitude value for every moisture mean profile curve. An inverse FFT was then performed after the filtering to return to the time domain. (Cooley and Tukey, 1965). An increase in either the frequency or corresponding amplitude, indicated conditions leading to higher fluctuations.

[Figure 3 about here.]

2.5. Quantification of effects and interactions of factors

The factor effects upon the responses from the experimental design derived from the CI-data and granule size measurements were estimated. Since multiple responses ($\bar{t}$, σ_θ^2, Pe, moisture entropy and GSD) were determined, it was helpful to fit a model simultaneously representing the variation of all responses to the variation and interactions of the factors. Therefore, using the Modde 10.1 software (Umetrics, Umeå, Sweden), partial least squares (PLS) modelling taking all responses simultaneously into account, was employed.

The effect plots are used to display the change in the response (y-axis) when each process factor (screw speed [RPM], material throughput [MFR], L/S [LSR], number of kneading discs [NK] and stagger angle [SA]) varies from its low to its high level, keeping all other factors at their center values of the interval (Fig.5 – 11). The y-axis indicates the estimated effect which has a value of twice the corresponding coefficients of the regression model. For each factor, the uncertainty of the effect is indicated by the 95% confidence interval error bar. When an interaction effect prevails, the synergistic or antagonistic effect of one factor depends on the level of another factor. The interaction effect represents the synergy or antagonism between two factors in explaining a response. In these plots the effects of factors on the response are sorted from the largest to the smallest. The factors and interaction terms with insignificant effect (those where the confidence interval includes zero) were removed from the model (Eriksson et al., 2000). Additionally, the interaction plot was used to display the predicted change in the response when one factor varies, and the second factor is set at both its low and high level, all other factors being set on their centre value. When in such a plot the two lines are parallel one can conclude that there is no interaction between the two factors, whereas when they cross each other there is a strong interaction. However, one should still be careful when interpreting the results, because sometimes, despite

the interaction between the factors, their effect on the response may not be significant, i.e. resulting only in a minor variation of the response.

3. Results and discussion

The performed design of experiments resulted in 51 residence time profiles (Fig. 4), and solid-liquid mixing and granulation performance results (see the overview of the performed experiments and obtained responses in the supplementary table S1). The power input variation was indicated by the measured torque in the granulator drive and the granulation time variation was expressed by the $\bar{t}$ (Fig. 5). The variation in axial mixing was derived from the width of the normalised RTD, i.e. the σ_θ^2 and the change in relative magnitude of convective and dispersive transport capacities was given by Pe (Fig. 8). The change in solid-liquid mixing of the bulk material was quantified as effect on MI. The frequency and amplitude of the mean moisture profiles quantified the dynamics in the solid-liquid mixing in the TSG (Fig. 10). To understand the role of process and screw design parameters on granulation performance, it is important to first discuss the observed effects of the factors on these responses (section 3.1-3.4). This will feed the detailed discussion to link granulation time and mixing performance with the resulting granulation yield in the follow-up section 3.5.

[Figure 4 about here.]

3.1. Change in torque at different process conditions

The torque of the granulator drive indicates the energy input to the granulation process by the motor drive. In this study, all the factors originating from the screw configuration and process conditions had a significant influence on the measured torque level (Fig. 5). This is in accordance with earlier studies on the effect of changing the process parameters on the torque level (Dhenge et al., 2010; Vercruysse et al., 2015; Kumar et al., 2014). An increase in the number of kneading discs most significantly increased the torque level and an increase

in L/S most significantly reduced the torque level. An increase in the material throughput resulted in higher torque. However, the material throughput had a significant interaction with L/S [LSR*MFR] (Fig. 6i). At a low material throughput increasing L/S resulted in an increased torque, whereas at a high material throughput increasing L/S resulted in a significant reduction in the torque. An increase in the screw speed led to a reduction of the torque. However, due to the interaction between L/S and the screw speed [LSR*RPM], a reduction in screw speed at a high L/S resulted in a sharp increase in the torque level compared to low L/S (Fig. 6ii). Increasing stagger angle resulted in a reduction of torque. However, this effect was found to be more pronounced at a low material throughput. At high material throughput, an elevated flow restriction by increasing stagger angle resulted in an increased torque level (Fig. 6iii). The interaction between the material throughput and screw speed [MFR*RPM], which impacts the fill ratio, resulted in a reduction of the torque when both screw speed and material throughput were increased simultaneously (Fig. 7i). At a low material throughput, this interaction did not exist. The highest torque level (12.41 N.m) was observed at a throughput of 25 kg/h, L/S of 6%, screw configuration with 12 kneading discs at 60° and screw speed of 500 rpm. The torque level was lowest (0.38 N.m) at a throughput of 25 kg/h, L/S of 8%, screw configuration with 4 kneading discs at 30° and screw speed of 900 rpm.

[Figure 5 about here.]

These observations suggest that the load on the screws (based on screw speed and material throughput) and the flow restriction (based on number of kneading discs and stagger angle) dictate the torque level of the granulator drive. Besides, at low barrel fill ratio, i.e. when the flow inertia is low, an increased moisture content at higher L/S causes sluggish flow and consequently higher torque. However, at a high throughput when more material is present, the inertial force is high and increasing L/S lubricates the granular flow leading to a reduc-

tion of the torque. The observed significant influence of all the factors on the torque level also suggests that the energy input to the system varied significantly for all the changes in process parameters. Thus, the studied experimental domain was suitable to investigate the effects of equipment and process parameters on other responses.

[Figure 6 about here.]

3.2. Granulation time at different process conditions

The granulation time in the TSG measured as $\bar{t}$ was most influenced by the screw speed and the number of kneading discs (Fig. 5). An increase in the screw speed resulted in a lower $\bar{t}$, i.e. the RTD profiles consistently shifted to the left in Fig. 4, whereas an increase in number of kneading discs led to an increase in the residence time. Increasing material throughput resulted in a reduction in the $\bar{t}$, which was also observed in earlier studies (Kumar et al., 2014; Dhenge et al., 2011). Additionally, $\bar{t}$ was significantly reduced by the interaction between material throughput and screw speed [MFR*RPM] (Fig. 7i). At a high fill ratio (i.e., increasing throughput at low screw speed) this interaction effect was dampened, but at lower fill ratio (i.e., increasing throughput at high screw speed), the $\bar{t}$ reduced significantly. An opposite effect on $\bar{t}$ was detected when more kneading discs were included in the screw configuration. An interaction between the number of kneading discs and the material throughput [MFR*NK] resulted in a significant reduction in the $\bar{t}$ when increasing the material throughput at a lower number of kneading discs (Fig. 7ii). Similarly, due to a significant interaction between the number of kneading discs and screw speed [NK*RPM], the $\bar{t}$ reduced when either the number of kneading discs was reduced at a low screw speed or screw speed was increased at a high number of kneading discs. Interestingly, an increasing L/S, which lowered the torque level of the granulator, resulted in an increase in $\bar{t}$. Although the effect of change in L/S on $\bar{t}$ was not very dominant, an increased sluggishness of powder

at high L/S and elevated flow restriction at higher stagger angle interacted to raise the $\bar{t}$. The maximum $\bar{t}$ (6.88 sec) was observed at a throughput of 25 kg/h, L/S of 8%, screw configuration with 12 kneading discs at 60° and screw speed of 500 rpm. The minimum $\bar{t}$ (1.61 sec) was observed at a throughput of 10 kg/h, L/S of 8%, screw configuration with 4 kneading discs at 60° and screw speed of 900 rpm.

[Figure 7 about here.]

These results suggest that at a given process condition, the required residence time for a good mixing and high granulation yield can mainly be achieved by either choosing the number of kneading discs in the screw configuration before starting the granulation process or by changing the screw speed during the process. Also, the reduction in $\bar{t}$ at low fill ratio indicates a synergy between throughput force and the drag force in the mixed flow condition. The lowering of torque level at a high L/S despite an increase in $\bar{t}$, i.e. more material inside the granulator, confirms that the granulation liquid at high fill ratio had a lubricating effect on the screw rotation without increasing the conveying rate.

3.3. Mixing at different process conditions

3.3.1. Axial mixing

The axial mixing during the bulk flow inside the granulator was quantified as σ_θ^2 and Pe (Fig. 8). Increasing the screw speed resulted in an increase in σ_θ^2, whereas a higher number of kneading discs resulted in reduced σ_θ^2. Visually this is reflected in a broadening of the RTD with increasing screw speed (Fig. 4). The opposite effect on the RTD profile was observed with increasing number of kneading discs. Similar results were also obtained in our previous experimental and model-based study (Kumar et al., 2014, 2015). Besides, an interaction between material throughput and the screw speed was observed such that increasing the

screw speed at a high material throughput, i.e. lowering the fill ratio, resulted in a high σ_θ^2 (Fig. 7i). However, keeping the material throughput at a high level when the screw speed was reduced resulted in a lower σ_θ^2 compared to the condition with low throughput and low screw speed. The largest σ_θ^2 (0.84) was observed at a throughput of 25 kg/h, L/S of 6%, screw configuration with 4 kneading discs at 60° and screw speed of 900 rpm. In contrast, the minimum σ_θ^2 (0.05) was observed at a throughput of 25 kg/h, L/S of 8%, screw configuration with 12 kneading discs at 60° and screw speed of 500 rpm.

Beside σ_θ^2 quantifying mainly dispersive transport, the Pe, which is the ratio of convective to dispersive transport in a system, was also directly influenced by the screw speed and the number of kneading discs. An increase in the screw speed resulted in the dominance of dispersive over convective transport phenomena, whereas the opposite effect was observed for increasing the number of kneading discs. Also, similar to σ_θ^2, the interaction between material throughput and the screw speed resulted in a fast reduction in Pe, i.e. dispersive transport increased when the screw speed was increased at a high throughput (Fig. 7i). This similarity in the effect of different factors on σ_θ^2 and Pe suggests that the dispersive transport change was significantly larger than the convective transport change when variations in the factors were introduced. At a low throughput, i.e. lower barrel filling, the observed increase in dispersive transport was lower compared to a high material throughput. Due to a significant interaction between stagger angle and screw speed, increasing screw speed resulted in a rapid decline in Pe at higher stagger angle (60°) compared to lower stagger angle (30°).

The largest Pe (36.66) was observed at a throughput of 25 kg/h, L/S of 8%, screw configuration with 12 kneading discs at 60° and screw speed of 500 rpm. In contrast, the minimum Pe (0.55), which is lower than 1 indicating that the dispersive transport length

was longer than the barrel size and exceeded the convective transport within the granulator barrel was observed at a throughput of 25 kg/h, L/S of 6%, screw configuration with 4 kneading discs at 60° and screw speed of 900 rpm.

[Figure 8 about here.]

These observations suggest that the flow regime inside the granulator is controlled both by the screw design and the process conditions. Due to the change in the hindrance to the axial flow by the fully filled zones around the kneading discs, dispersive transport was less efficient for a high number of kneading discs. Increasing the throughput force and drag force by the increasing material throughput and screw speed simultaneously and consequently a low fill ratio led to an increase in the wall slippage resulting in more axial mixing in the TSG.

3.3.2. Solid-liquid mixing

The solid-liquid mixing in the bulk mixture was quantified as MI and its dynamics during continuous granulation were quantified as frequency and amplitude of the mean moisture profile of each run. According to the effect plot for the MI, the bulk mixing was most significantly reduced by the increase in material throughput (Fig. 10). In contrast, increasing the number of kneading discs significantly increased the bulk mixing, which is reflected by an increase in the mixing index. Also the throughput and the number of kneading discs interacted [MFR*NK] significantly leading to an increase in the MI at a high throughput by the increasing number of kneading discs (Fig. 7ii). Additionally, MI increased significantly at a high L/S. The effect of a change in L/S also had significant interaction with the changes in material throughput. An increase in the material throughput at low L/S resulted in a lower MI than when a high L/S is applied. The effect of a change in the screw speed was not significant on the MI but its interaction with the change in the number of kneading

discs resulted in a significant reduction in MI when the screw speed was increased at a high number of kneading discs (Fig. 9i). The stagger angle did not affect the MI significantly. The highest MI (0.39) was observed at a throughput of 25 kg/h, L/S of 8%, screw configuration with 12 kneading discs at 30° and screw speed of 500 rpm. In contrast, the minimum MI (0.13) was observed at a throughput of 25 kg/h, L/S of 8%, screw configuration with 4 kneading discs at 60° and a screw speed of 900 rpm.

[Figure 9 about here.]

The effect plot for the frequency of mean moisture profile showed that, similar to the bulk mixing, increasing the material throughput increased the frequency of the mean moisture profile, i.e. indicating inferior solid-liquid mixing. The opposite effect occurred when the number of kneading discs increased (Fig. 10). Also, an interaction between the throughput and number of kneading discs [MFR*NK] significantly influenced MI. An increase in the material throughput at a high number of kneading discs resulted in an increase in the frequency, thus more variations in the dynamic profile, which is opposite to the observation for the bulk mixing as indicated by MI (Fig. 7ii). Additionally, due to a significant interaction between the material throughput and stagger angle [MFR*SA], the frequency of the mean moisture profile increased more rapidly by the increasing throughput at a high stagger angle (60°) compared to a low stagger angle (30°) between kneading discs (Fig. 6iii). Moreover, the interaction between the stagger angle and number of kneading discs in the screw configuration at a low number of kneading discs resulted in an increase in frequency when the stagger angle was increased. The opposite was observed when the stagger angle was increased at a high number of kneading discs. The change in L/S, screw speed and stagger angle had no significant effect on the variation frequency.

The effect plot for the amplitude of the mean moisture profile also showed that similar

to the bulk mixing, the material throughput most significantly resulted in a decrease in the degree of variation. However, an increase in the number of kneading discs, screw speed and stagger angle equally resulted in an increase in the variation and, hence, a higher amplitude. A high L/S caused a reduction in the extent of fluctuation, i.e. a lower amplitude. Due to the interaction between the material throughput and L/S [MFR*LSR], an increase in the L/S resulted in a lower amplitude when the material throughput was increased.

These results suggest that although a high material throughput and a high screw speed are desired for process efficiency, their exclusive increase may cause inefficient solid-liquid mixing which will result in an inferior granulation yield. Similarly, an increase in the number of kneading discs should be considered to obtain good solid-liquid mixing by reducing both the rate and degree of variations in the moisture content of the granules. Also, at a higher L/S, bulk mixing is better and the degree of variation is less, indicating that a proper amount of liquid addition is also required for good distribution of the liquid during granulation. However, this improvement in solid-liquid mixing at high L/S also suggests an active role of the pumping rate on the solid-liquid mixing. The effects of fluctuating pressure and varation in the fluid flow by the perstaltic pump can be better compensated by the axial mixing as this variation period is much smaller (i.e., high frequency) compared to the residence time of the material in the TSG. In contrast, granulation liquid inflow variations at a low frequency cannot be easily compensated by the axial mixing due to the small residence time of the material in the TSG. Similar significant variations in the moisture content distribution were earlier observed by Vercruysse et al. (2013), and are thus critical to the granulator design.

[Figure 10 about here.]

3.4. GSD at different process conditions

In order to understand the effect of each factor on the GSD, the sieved granules were classified in three fractions (fine (<150 µm), yield (150-1400 µm) and oversized (>1400 µm)) (Fig. 11). An increase in L/S and number of kneading discs resulted in a lower amount of fines in the produced granules. On the other hand, an increase in the stagger angle and screw speed led to more fines in the granules. Although material throughput independently had no significant influence on the fines fraction, a significant interaction between material throughput and the number of kneading discs [MFR*NK] resulted in a more rapid reduction in the amount of fines with increasing number of kneading discs at high throughput (Fig. 7ii). Also, the two factors with an opposite effect on fines i.e., the number of kneading discs and the screw speed interacted significantly [NK*RPM]. The amount of fines at a low number of kneading discs and a high screw speed was less, but the opposite was observed when high screw speed was applied along with a high number of kneading discs (Fig. 9i). The maximum amount of fines (55.0% when the yield and oversized fractions were 42.0 and 3.0 % respectively) was observed at a throughput of 10 kg/h, L/S of 6%, screw configuration with 12 kneading discs at 30° and a screw speed of 900 rpm. In contrast, the smallest amount of fines (4.9% when the yield and oversized fractions were 41.7 and 53.4 % respectively) was observed at a throughput of 25 kg/h, L/S of 8%, screw configuration with 12 kneading discs at 30° and a screw speed of 500 rpm.

The yield fraction was most significantly influenced by the screw speed and the material throughput (Fig. 11). A higher screw speed resulted in an increase of the yield fraction, whereas increasing the material throughput resulted in a reduction of the yield fraction. Additionally, an increase in stagger angle resulted in a reduction in the yield fraction and the opposite was observed when L/S was increased. A strong interaction between the number of kneading discs and the screw speed resulted in a decrease in the yield fraction when the number of kneading discs was increased at a high screw speed (Fig. 9i). The yield frac-

tion increased when the number of kneading discs was increased at low screw speed. This indicates that an increase in the mechanical shear beyond a certain extent is not favourable to the granulation yield. Similarly, due to interaction between material throughput and number of kneading discs [MFR*NK], more yield fraction granules were produced when the number of kneading discs was increased at high throughput (Fig. 7ii). The change in yield fraction was also influenced by the interaction of material throughput with stagger angle and screw speed. Increasing the throughput at lower stagger angle resulted in a drastic reduction in the yield fraction (Fig. 6iii). Increasing the screw speed at a low throughput increased the yield fraction more than operation at a high throughput (Fig. 7i). The highest yield fraction (62.9% when the fines and oversized fractions were 18.8 and 18.2 % respectively) was observed at a throughput of 25 kg/h, L/S of 6%, screw configuration with 12 kneading discs at 60° and a screw speed of 500 rpm. In contrast, the lowest yield fraction (41.7% when the fines and oversized fractions were 4.9 and 53.4 % respectively) was observed at a throughput of 25 kg/h, L/S of 8%, screw configuration with 12 kneading discs at 30° and a screw speed of 500 rpm.

The effect plot for the oversized fraction shows that the additional liquid at a high L/S significantly increased the amount of oversized granules (Fig. 11). Similarly, increasing the number of kneading discs and the material throughput also resulted in increased production of oversized granules. This suggests ineffective mixing by the kneading discs despite an increase in the number of kneading discs. However, increasing stagger angle and screw speed lowered the oversized fraction. An interaction between L/S and stagger angle resulted in a rapid increase in the oversized fraction at low L/S when the stagger angle was reduced from 60° to 30° (Fig. 9ii). Additionally, the interaction between L/S and screw speed resulted in a reduction in the oversized fraction at high L/S when the screw speed was increased (Fig. 6ii). The highest fraction of oversized granules (53.4% when the fines and yield frac-

tions were 4.9 and 41.7 % respectively) was observed at a throughput of 25 kg/h, L/S of 8%, screw configuration with 12 kneading discs at 30° and a screw speed of 500 rpm. The smallest oversized granule fraction (3% when the fines and yield fractions were 55.0 and 42.0 % respectively) was observed at a throughput of 10 kg/h, L/S of 6%, screw configuration with 12 kneading discs at 30° and a screw speed of 900 rpm.

[Figure 11 about here.]

3.5. Link between granulation time, mixing and yield

The purpose of granulation process design and optimisation is to maximize the process efficiency, i.e. maximising the yield fraction. The results discussed so far (section 3.1 - 3.4) suggest a correlation between the granulation time, mixing and the GSD. This was also reflected by the PLS loadings plot (Fig. 12). The measured torque of the granulator drive indicating power input to the system, Pe quantifying the axial mixing, MI quantifying the solid-liquid mixing and $\bar{t}$ quantifying average time spent by the material inside the granulator are positively correlated as can be seen in the loadings plot. On the other hand, all the three size fractions (fine, yield and oversized granules) are located in different regions suggesting that they have different important contributing factors. Moreover, the desired condition for the responses such as a high residence time, a good axial as well as solid-liquid mixing and resulting high yield fraction are favoured by different factors. Therefore, the connections between different factors and responses requires detailed discussion.

[Figure 12 about here.]

As discussed in the introduction, due to the short residence time, the major challenge in twin-screw wet granulation is to achieve proper solid-liquid mixing in the shortest distance along the granulator screw to allow more time for other constitutive mechanisms of

granulation to shape the final distribution. For this purpose, kneading discs were used in the TSG which improved solid-liquid mixing both by increasing the bulk mixing and reducing the frequency of deviations in the moisture content of the granules (Fig. 10). A high number of kneading discs also resulted in a relatively longer residence time. Despite this improvement in mixing and time, increasing the number of kneading discs did not significantly contribute to an increased yield fraction (Fig. 11). Additionally, increasing the L/S had no significant contribution to increasing the desired yield fraction since most of the additional liquid resulted in the formation of oversized granules. This evidently indicates that despite the contribution of kneading discs in the solid-liquid mixing, the required quality of mixing inside the TSG barrel was still not achieved. Since the highest torque level (12.4 N.m) was also observed by the screw configuration with 12 kneading discs at 60° and a screw speed of 500 rpm, further increase in the number of kneading discs will for sure increase the bulk mixing, but on the other hand significantly limit the operational ranges of the process settings. Therefore, more efforts should be done to modify the TSG screw configuration both using conventional (conveying and kneading elements) as well as non-conventional screw elements with modified geometries to improve the solid-liquid mixing (Vercruysse et al., 2015; Sayin et al., 2015; Meier et al., 2015). Moreover, the liquid feeding system in the TSGs should be improved to prevent variations in granulation liquid inflow with a period larger than the mean residence time of the material as discussed earlier in section 3.3.2. Instead of peristaltic pumps which are being used currently and cause pulsating flow, a constant flow pump, such as dual piston pump, should be used.

Increasing the screw speed not only lowered the torque, allowing greater flexibility in choosing process settings but also most significantly increased the yield fraction of the granules despite smaller $\bar{t}$. However, mixing at a high screw speed was more dispersive as indicated by Pe than the bulk mixing indicated by MI (Fig. 8 and 10). Due to this, the fines fraction

increased as well. Increasing the material throughput (which will be the ultimate target in industrial production) quickly changed the flow regime inside the granulator which consequently reduced the yield fraction. Moreover, beside reducing the axial mixing, an increasing material throughput also reduced the bulk mixing which was mostly driven by the distributive mixing by the kneading discs. Since the number of kneading discs significantly interacts both with material throughput and screw speed, keeping the number of kneading discs at a fixed level, a balance between material throughput and screw speed should be strived for in order to achieve the required granulation time, axial mixing and solid-liquid mixing for a high granulation yield. Moreover, although increasing stagger angle had a negative effect on yield fraction, since increasing the stagger angle and screw speed simultaneously, lowered both fines and the oversized fraction in the granules produced, the higher stagger angle (60°) should be used in the screw configuration.

Additionally, considering the inability of experimental studies in visualising and measuring the effects of screw configuration and elements on powder flow, mixing and granulation rate processes at particle-scale, further studies based on application of mechanistic modelling tools, such as discrete element simulations and population balance modelling should be performed to improve the understanding of the governing constitutive mechanisms of the twin-screw wet granulation process. These mechanistic tools can also be used for exploring the effect of changes in the granulator screw design and the liquid addition strategy for an improvement in the liquid distribution and consequently obtaining a higher wet granulation yield.

4. Conclusions

NIR chemical imaging was shown to be an adequate tool for simultaneous characterisation of the material flow, axial mixing and bulk mixing analysis during twin-screw granulation. This also allowed investigating the effect of RTD and solid-liquid mixing on the resulting GSD to better understand the overall influence on different flow and mixing conditions. According to the study, an interaction between screw speed, the material throughput, liquid-to-solid ratio, number of kneading discs and stagger angle led to variation in the residence time as well as mixing capacity. At a high screw speed, despite high axial mixing leading to reduction of the oversized (>1400 µm) fraction and a higher yield fraction, a low residence time resulted in increase in the fine (<150 µm) fraction. Similarly, increasing L/S led to more oversized granules, which increased further at higher throughput. This indicated insufficient solid-liquid mixing capacity of the current kneading discs which is ultimately required for good granulation performance. Similarly, at high throughput improper solid-liquid mixing resulted in more oversized particles. Thus, a balance between material throughput and screw speed should be looked for to achieve the required granulation time and solid-liquid mixing for high granulation yield. Additionally, more efforts should be done both to modify the screw configuration as well as geometry of the mixing elements to improve the mixing capacity of the TSG. The results from this experimental study improved the understanding regarding the interplay between granulation time, the axial and the solid-liquid mixing responsible for the granulation yield. However, only empirical qualitative insight is gained, not detailed quantitative insight. Therefore, application of mechanistic modelling tools, such as discrete element simulations and population balance modelling, needs to be further explored for further detailed investigation of material flow and mixing and their impact on granulation yield during twin-screw granulation.

Acknowledgements

Financial support for this research from the BOF (Bijzonder Onderzoeksfonds Universiteit Gent, Research Fund Ghent University) is gratefully acknowledged.

References

Cooley, J. W., Tukey, J. W., 1965. An algorithm for the machine calculation of complex Fourier series. Math. Comput. 19, 297–301.

Dhenge, R. M., Cartwright, J. J., Doughty, D. G., Hounslow, M. J., Salman, A. D., 2011. Twin screw wet granulation: Effect of powder feed rate. Adv. Powder Technol. 22 (2), 162 – 166.

Dhenge, R. M., Fyles, R. S., Cartwright, J. J., Doughty, D. G., Hounslow, M. J., Salman, A. D., 2010. Twin screw wet granulation: Granule properties. Chem. Eng. J. 164 (2-3), 322–329, Pharmaceutical Granulation and Processing.

El Hagrasy, A., Hennenkamp, J., Burke, M., Cartwright, J., Litster, J., 2013. Twin screw wet granulation: Influence of formulation parameters on granule properties and growth behavior. Powder Technol. 238, 108–115.

Eriksson, L., Johansson, E., Kettaneh-Wold, N., Wikström, C., Wold, S., 2000. Design of Experiments -Principles and Applications. Umetrics Academy.

Fogler, H., 2006. Elements Of Chemical Reaction Engineering. Pearson international edition. Prentice Hall Professional Technical Reference.

Guida, A., Nienow, A. W., Barigou, M., 2010. Shannon entropy for local and global description of mixing by lagrangian particle tracking. Chem. Eng. Sci. 65 (10), 2865–2883.

Kumar, A., Gernaey, K. V., De Beer, T., Nopens, I., 2013. Model-based analysis of high shear wet granulation from batch to continuous processes in pharmaceutical production – a critical review. Eur. J. Pharm. Biopharm. 85 (3, Part B), 814 – 832.

Kumar, A., Vercruysse, J., Toiviainen, M., Panouillot, P.-E., Juuti, M., Vanhoorne, V., Vervaet, C., Remon, J. P., Gernaey, K. V., De Beer, T., Nopens, I., 2014. Mixing and transport during pharmaceutical twin-screw wet granulation: Experimental analysis via chemical imaging. Eur. J. Pharm. Biopharm. 87 (2), 279 – 289.

Kumar, A., Vercruysse, J., Vanhoorne, V., Toiviainen, M., Panouillot, P.-E., Juuti, M., Vervaet, C., Remon, J. P., Gernaey, K. V., De Beer, T., Nopens, I., 2015. Conceptual framework for model-based analysis of residence time distribution in twin-screw granulation. Eur. J. Pharm. Sci. 71 (0), 25 – 34.

Lee, K. T., Ingram, A., Rowson, N. A., Aug. 2012. Twin screw wet granulation: the study of a continuous

twin screw granulator using Positron Emission Particle Tracking (PEPT) technique. Eur. J. Pharm. Biopharm. 81 (3), 666–73.

Li, H., Thompson, M., O'Donnell, K., 2014. Understanding wet granulation in the kneading block of twin screw extruders. Chem. Eng. Sci. 113 (0), 11 – 21.

Meier, R., Thommes, M., Rasenack, N., Krumme, M., Moll, K.-P., Kleinebudde, P., 2015. Simplified formulations with high drug loads for continuous twin-screw granulation. Int. J. Pharm. (0), –.

Poechlauer, P., Manley, J., Broxterman, R., Gregertsen, B., Ridemark, M., 2012. Continuous processing in the manufacture of active pharmaceutical ingredients and finished dosage forms: An industry perspective. Org. Process Res. Dev. 16 (10), 1586–1590.

Sayin, R., Hagrasy, A. E., Litster, J., 2015. Distributive mixing elements: Towards improved granule attributes from a twin screw granulation process. Chemical Engineering Science 125 (0), 165 – 175, pharmaceutical Particles and Processing.

Van Melkebeke, B., Vervaet, C., Remon, J. P., 2008. Validation of a continuous granulation process using a twin-screw extruder. Int. J. Pharm. 356 (1-2), 224–230.

Vercruysse, J., Burggraeve, A., Fonteyne, M., Cappuyns, P., Delaet, U., Assche, I. V., Beer, T. D., Remon, J., Vervaet, C., 2015. Impact of screw configuration on the particle size distribution of granules produced by twin screw granulation. Int. J. Pharm. 479 (1), 171 – 180.

Vercruysse, J., Toiviainen, M., Fonteyne, M., Helkimo, N., Ketolainen, J., Juuti, M., Delaet, U., Assche, I. V., Remon, J. P., Vervaet, C., De Beer, T., 2013. Visualization and understanding of the granulation liquid mixing and distribution during continuous twin screw granulation using NIR chemical imaging. Eur. J. Pharm. Biopharm. 86 (3), 383–392.

List of Figures

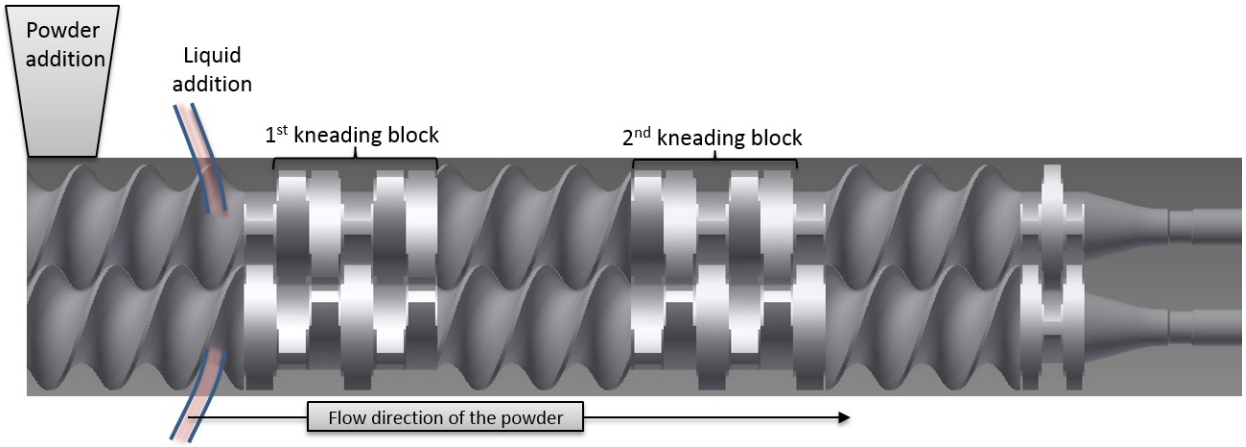

Figure 1: Screw configuration with 12 kneading discs (2 blocks) used in the twin-screw granulator during the study.

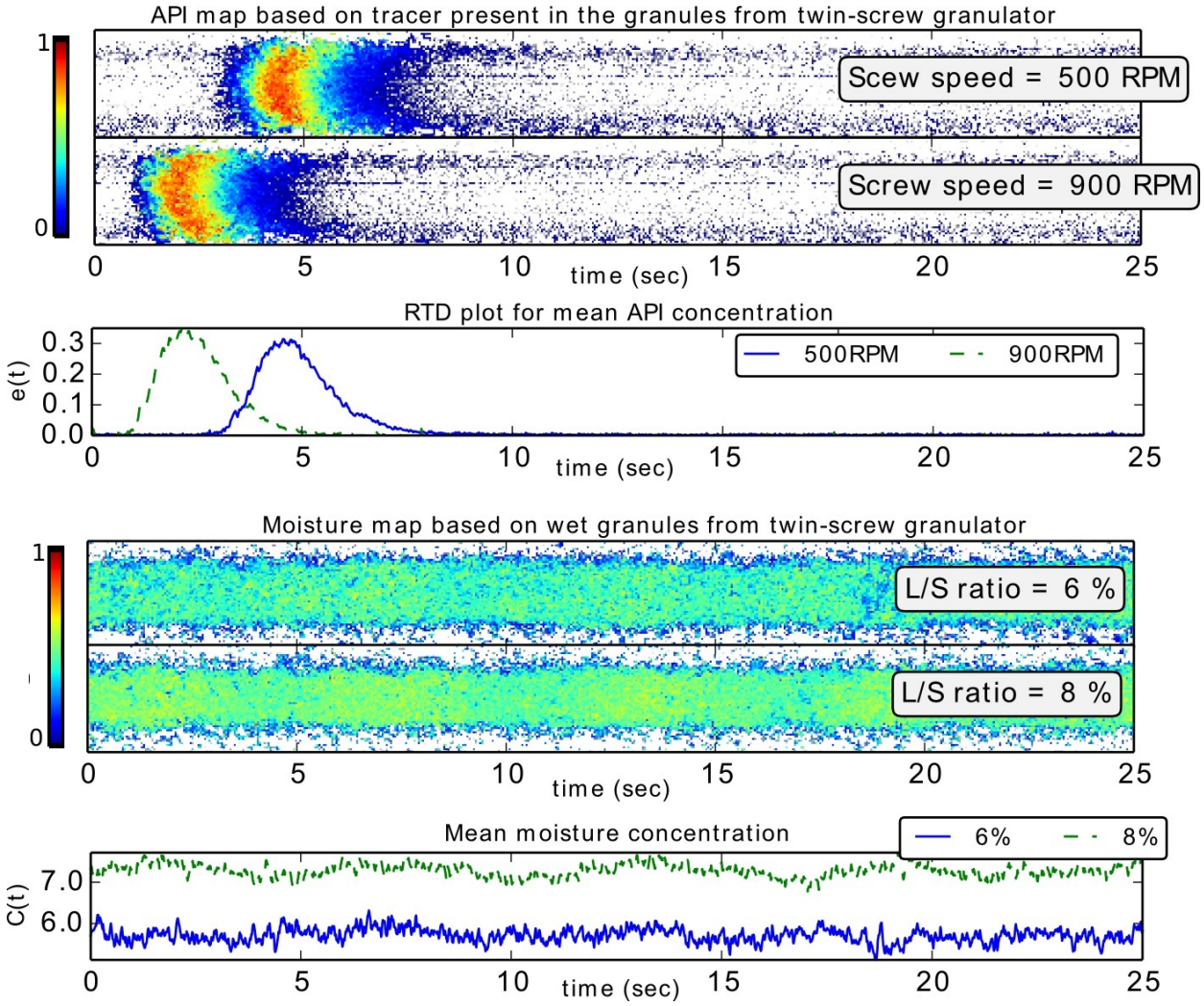

Figure 2: Representation of an active pharmaceutical ingredient (API)-map and a moisture map, the corresponding mean temporal profile, which were translated into the corresponding residence time distribution and moisture distribution for the twin screw granulator at fixed material throughput (25 kg/h), number of kneading discs (6), stagger angle (60°) and different screw speeds.

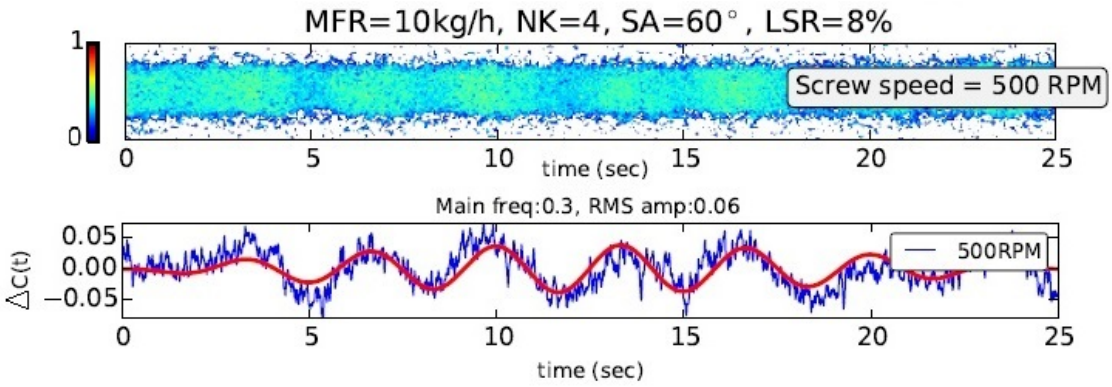

Figure 3: The FFT algorithm was used to remove noise from the mean moisture profiles, allowing the identification of the most dominant frequency band and corresponding amplitude.

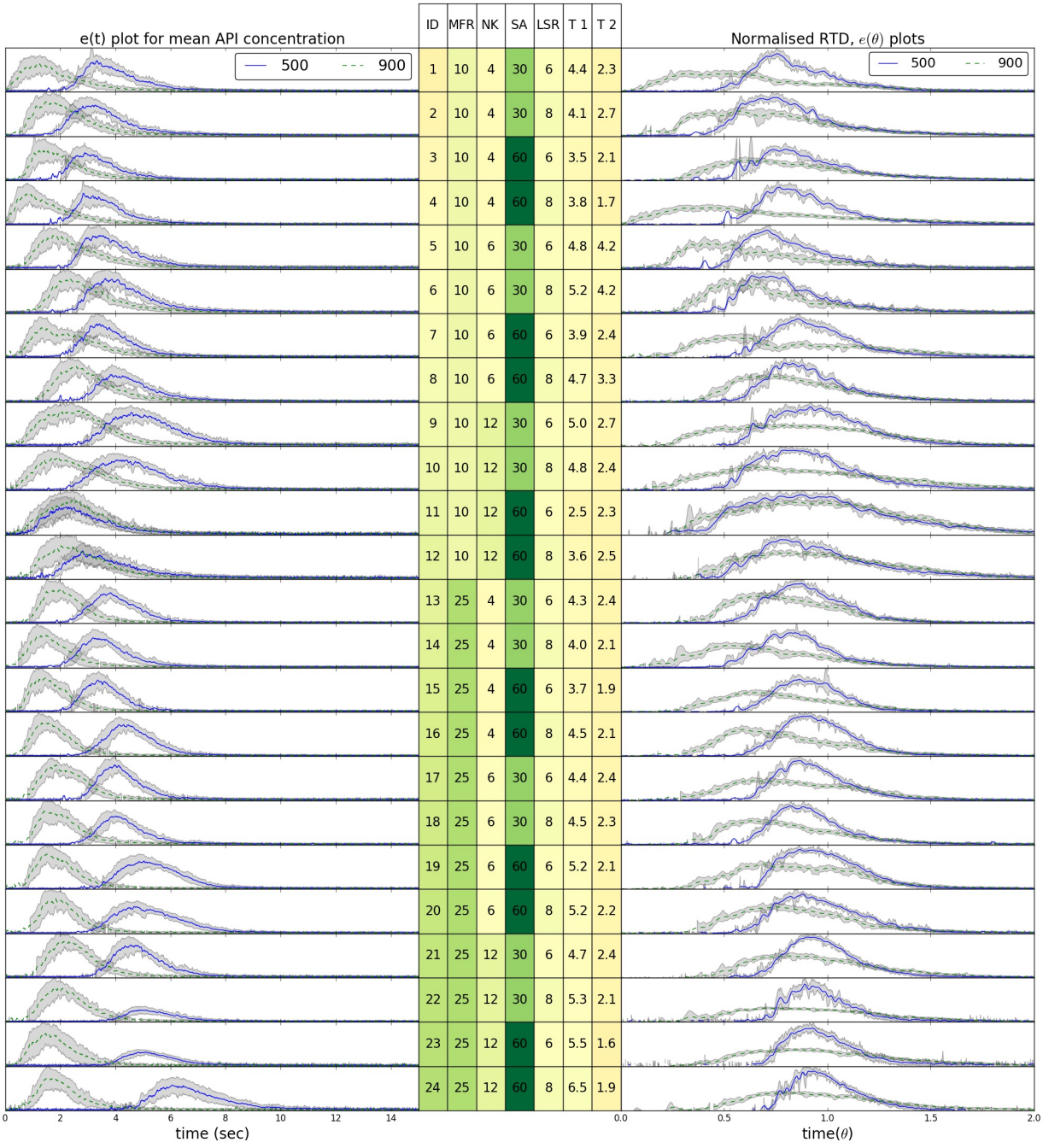

ID	MFR	NK	SA	LSR	T 1	T 2
1	10	4	30	6	4.4	2.3
2	10	4	30	8	4.1	2.7
3	10	4	60	6	3.5	2.1
4	10	4	60	8	3.8	1.7
5	10	6	30	6	4.8	4.2
6	10	6	30	8	5.2	4.2
7	10	6	60	6	3.9	2.4
8	10	6	60	8	4.7	3.3
9	10	12	30	6	5.0	2.7
10	10	12	30	8	4.8	2.4
11	10	12	60	6	2.5	2.3
12	10	12	60	8	3.6	2.5
13	25	4	30	6	4.3	2.4
14	25	4	30	8	4.0	2.1
15	25	4	60	6	3.7	1.9
16	25	4	60	8	4.5	2.1
17	25	6	30	6	4.4	2.4
18	25	6	30	8	4.5	2.3
19	25	6	60	6	5.2	2.1
20	25	6	60	8	5.2	2.2
21	25	12	30	6	4.7	2.4
22	25	12	30	8	5.3	2.1
23	25	12	60	6	5.5	1.6
24	25	12	60	8	6.5	1.9

Figure 4: The age distribution (left) and normalised RTD (right) profiles with a shaded region denoting the standard deviation at different screw speed (500, 900 RPM) during various experiments (ID) using twin screw granulation [SA: stagger angle (°), NK: number of kneading discs (-), MFR: material throughput (kg/h), LSR: liquid-solid ratio (%), T 1: mean residence time at 500 RPM (s), T 2: mean residence time at 900 RPM (s)].

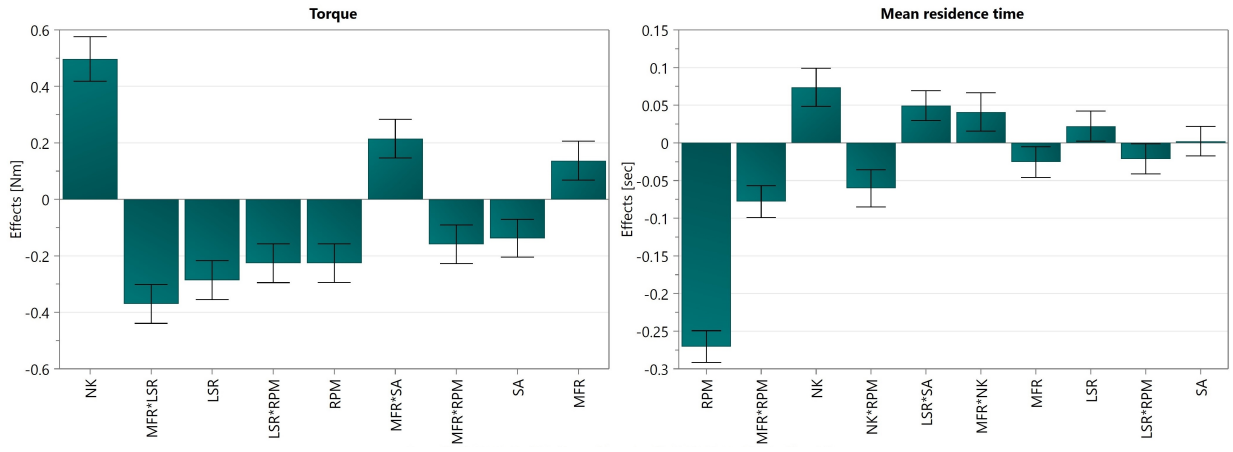

Figure 5: Effects plots showing predicted changes in the measured torque [N=42; DF=32; R2=0.95] and mean residence time [N=41; DF=30; R2=0.97] when factors, number of kneading discs (NK) [4, 6, 12], screw speed (RPM) [500-900 rpm], throughput (MFR) [10-25 kg/h], liquid-to-solid ratio (LSR) [6-8%] and stagger angle (SA) [30-60°], vary from the low to the high level, while keeping the other factors at their center point value (confidence level=0.95).

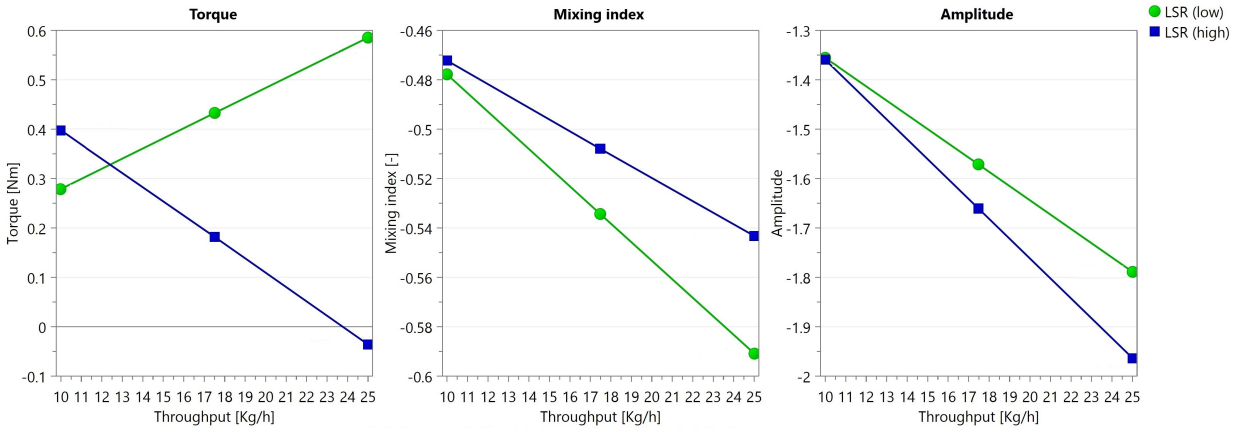

(i) Predicted changes in the measured torque, MI and amplitude of the mean moisture profile.

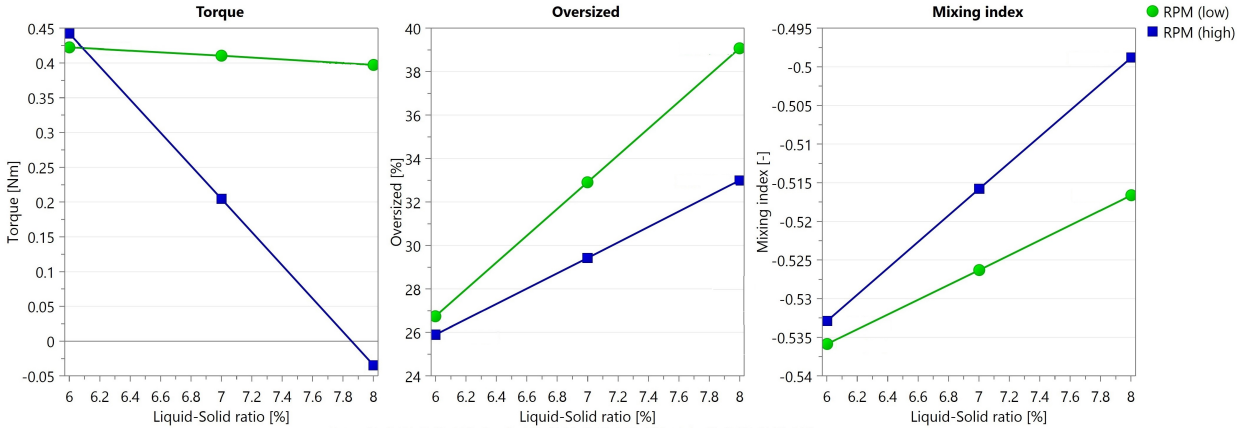

(ii) Predicted changes in the measured torque, oversized fraction of granules (>1400 µm) and mixing index (MI).

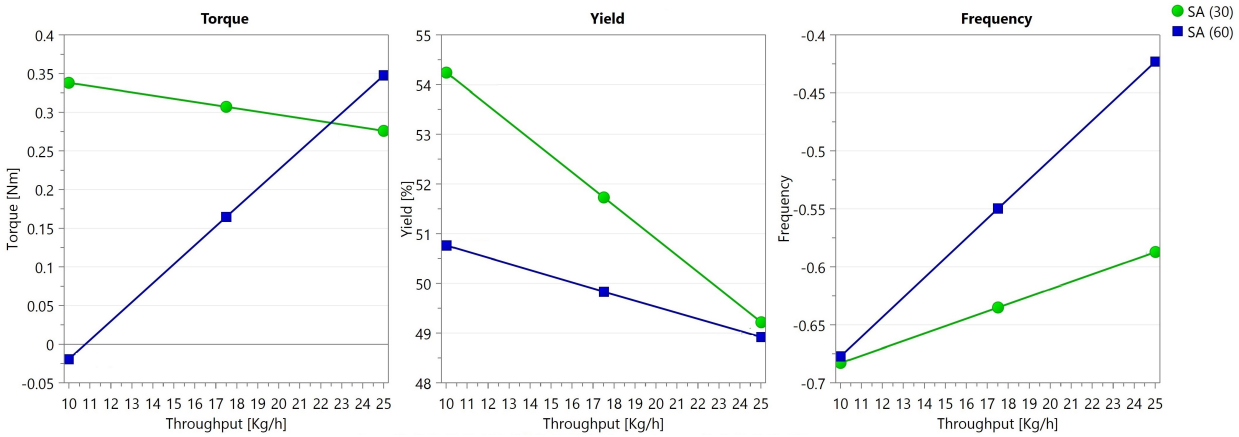

(iii) Predicted changes in the measured torque, yield fraction (>150µm to <1400 µm) of granules and frequency of the mean moisture profile.

Figure 6: Predicted changes in the responses due to interaction (i) between the liquid-to-solid ratio (L/S) and material throughput [MFR*LSR], (ii) between the liquid-to-solid ratio (L/S) and screw speed [LSR*RPM] and (iii) between the material throughput and stagger angle [MFR*SA] in the screw configuration.

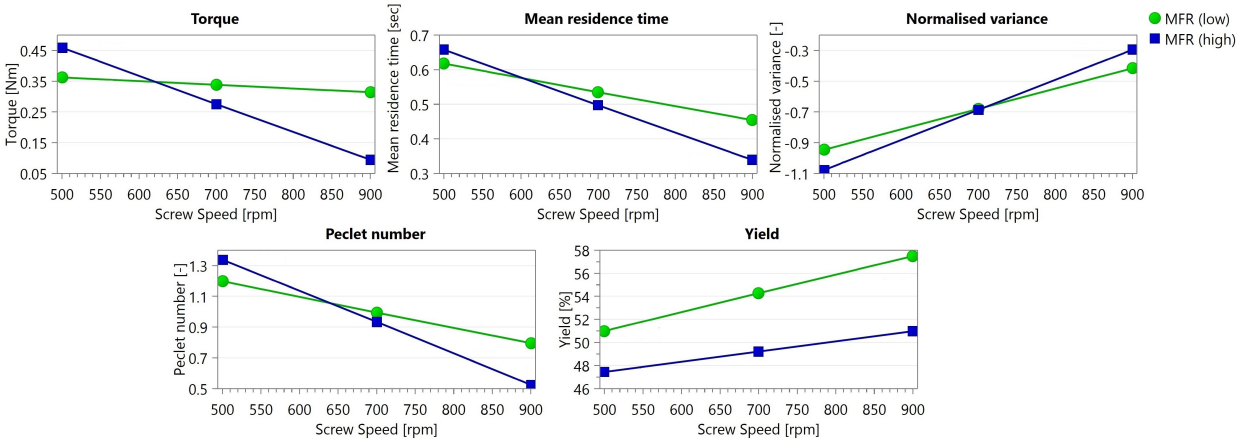

(i) Predicted changes in the measured torque, mean residence time, Pe and yield fraction (>150 µm to <1400 µm) of granules, mixing index (MI) and frequency of the mean moisture profiles.

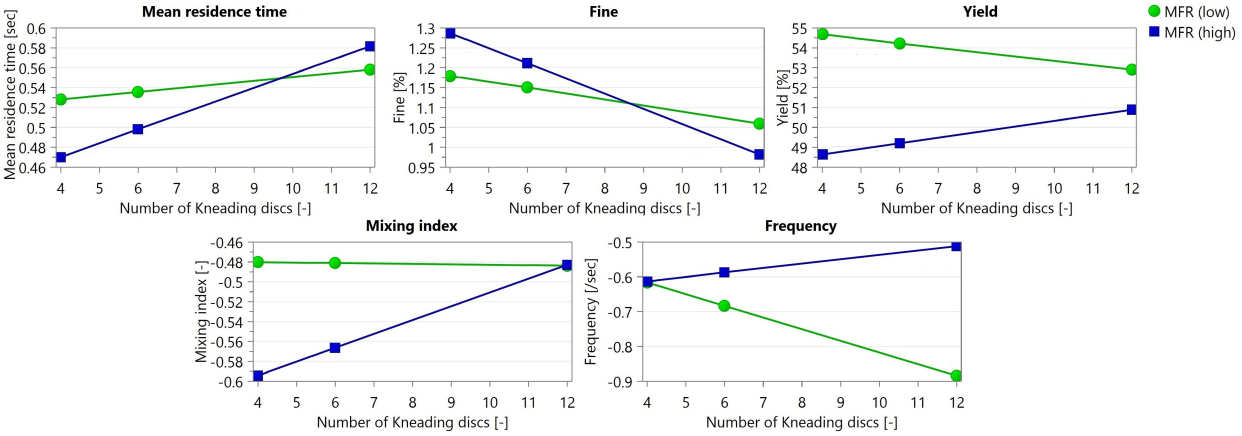

(ii) Predicted changes in the mean residence time,and fine (<150 µm) and yield fractions (>150 µm to <1400 µm) of granules.

Figure 7: Predicted changes in the responses due to interaction (a) between the material throughput and screw speed [MFR*RPM] and (b) between material throughput and number of kneading discs [MFR*NK] in the screw configuration.

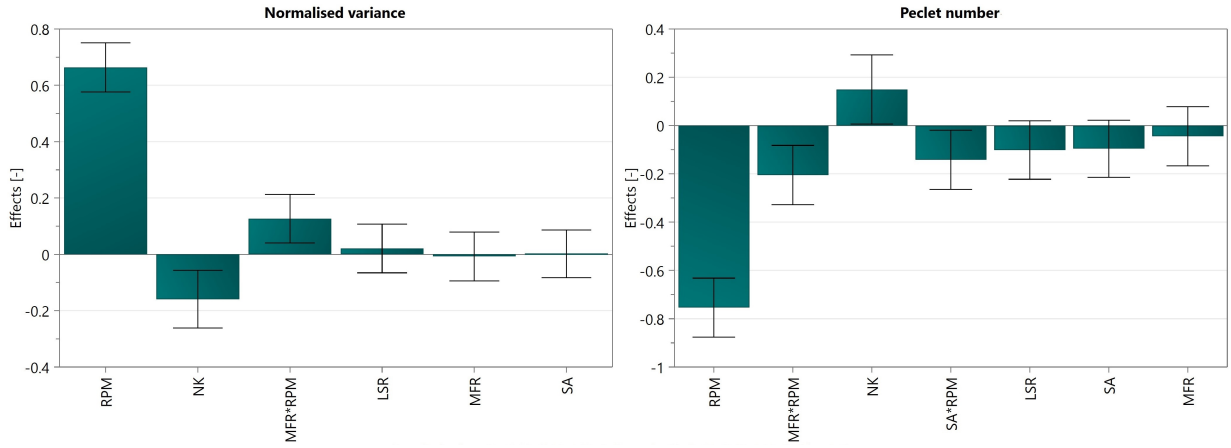

Figure 8: Effects plots showing predicted changes in the mean centered variance [N=46; DF=39; R2=0.87] and Péclet number [N=43; DF=35; R2=0.84] when factors, number of kneading discs (NK) [4, 6, 12], screw speed (RPM) [500-900 rpm], throughput (MFR) [10-25 kg/h], liquid-to-solid ratio (LSR) [6-8%] and stagger angle (SA) [30-60°], vary from a low to a high level, while keeping the other factors at their center point value (confidence level=0.95).

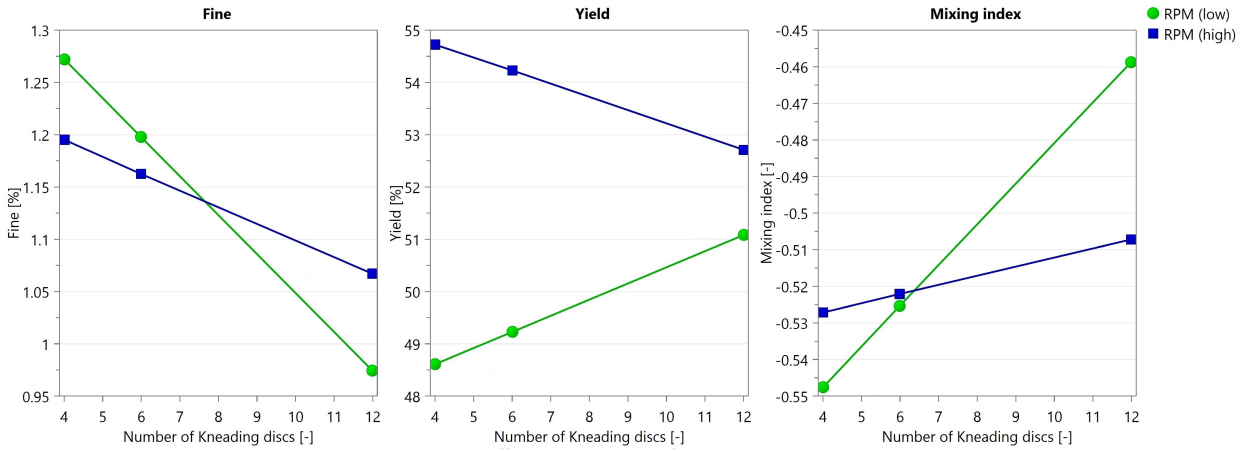

(i) Predicted changes in the mean residence time, and fine (<150 µm) and yield fractions (>150 µm to <1400 µm) of granules.

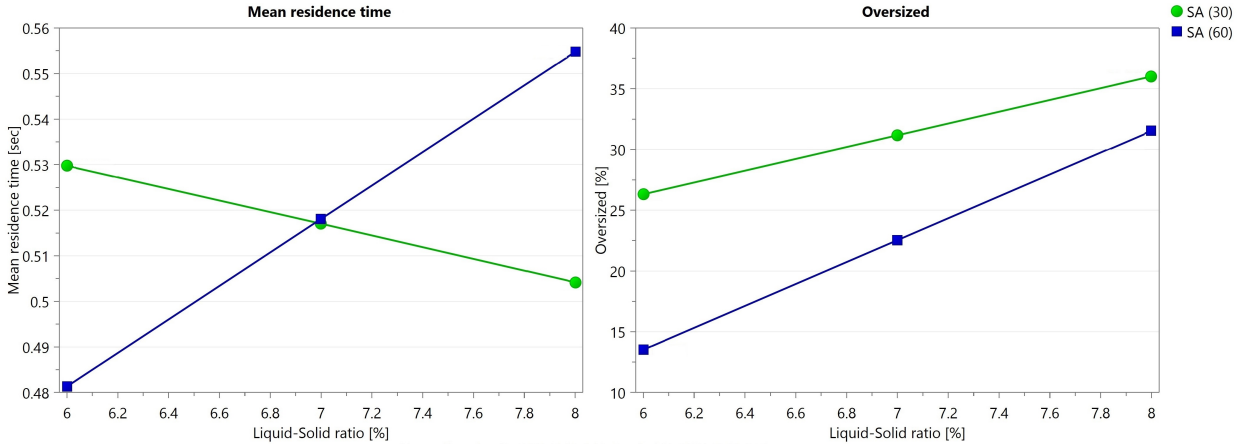

(ii) Predicted changes in the mean residence time, and oversized granule fraction (>1400 µm).

Figure 9: Predicted changes in the responses due to interaction (i) between number of kneading discs and screw speed [NK*RPM], and (i) between liquid-to-solid ratio and stagger angle between kneading discs [LSR*SA] in the screw configuration.

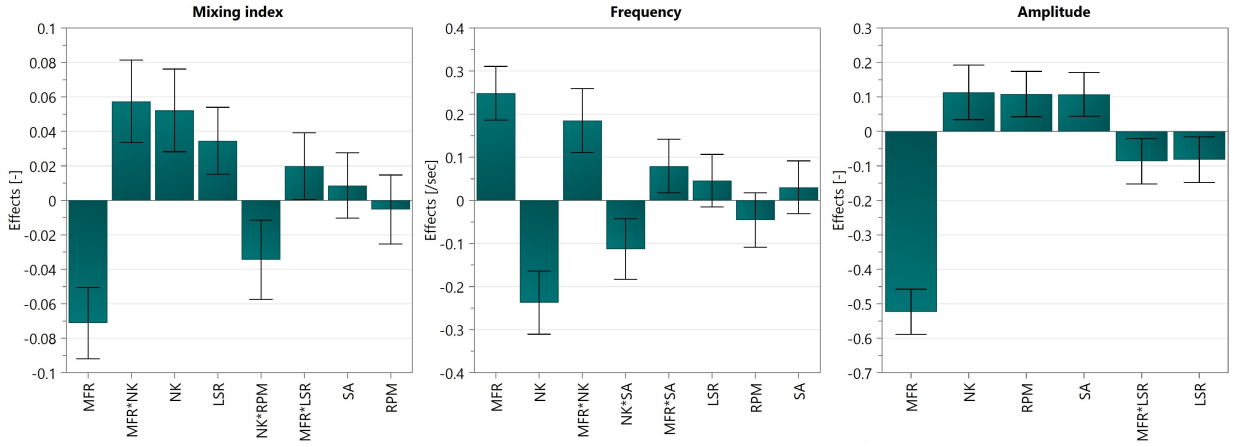

Figure 10: Effects plots showing predicted changes in the Shannon entropy based mixing index (MI) [N=43; DF=34; R2=0.80], frequency [N=41; DF=32; R2=0.84] and amplitude [N=45; DF=38; R2=0.88] of the mean moisture profiles when factors, number of kneading discs (NK) [4, 6, 12], screw speed (RPM) [500-900 rpm], throughput (MFR) [10-25 kg/h], liquid-to-solid ratio (LSR) [6-8%] and stagger angle (SA) [30-60°], vary from a low to a high level, while keeping the other factors at their center point value (confidence level=0.95).

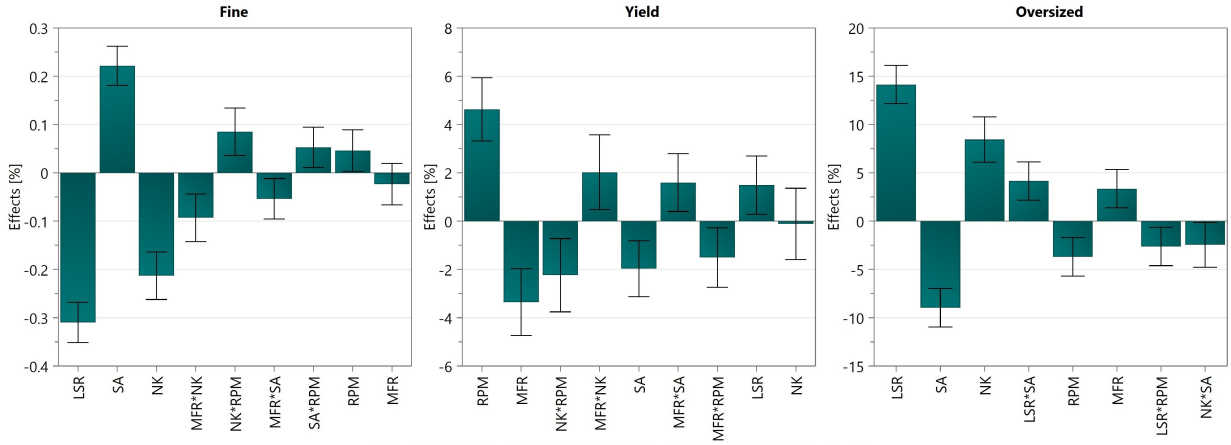

Figure 11: Effects plots showing predicted changes in the fines (>150 µm) [N=49; DF=39; R2=0.93], yield [150-1400 µm] [N=38; DF=28; R2=0.84] and oversized (>1400 µm) [N=47; DF=38; R2=0.92] fractions of the resulting GSD produced when factors, number of kneading discs (NK) [4, 6, 12], screw speed (RPM) [500-900 rpm], throughput (MFR) [10-25 kg/h], liquid-to-solid ratio (LSR) [6-8%] and stagger angle (SA) [30-60°], vary from a low to a high level, while keeping the other factors at their center point value (confidence level=0.95).

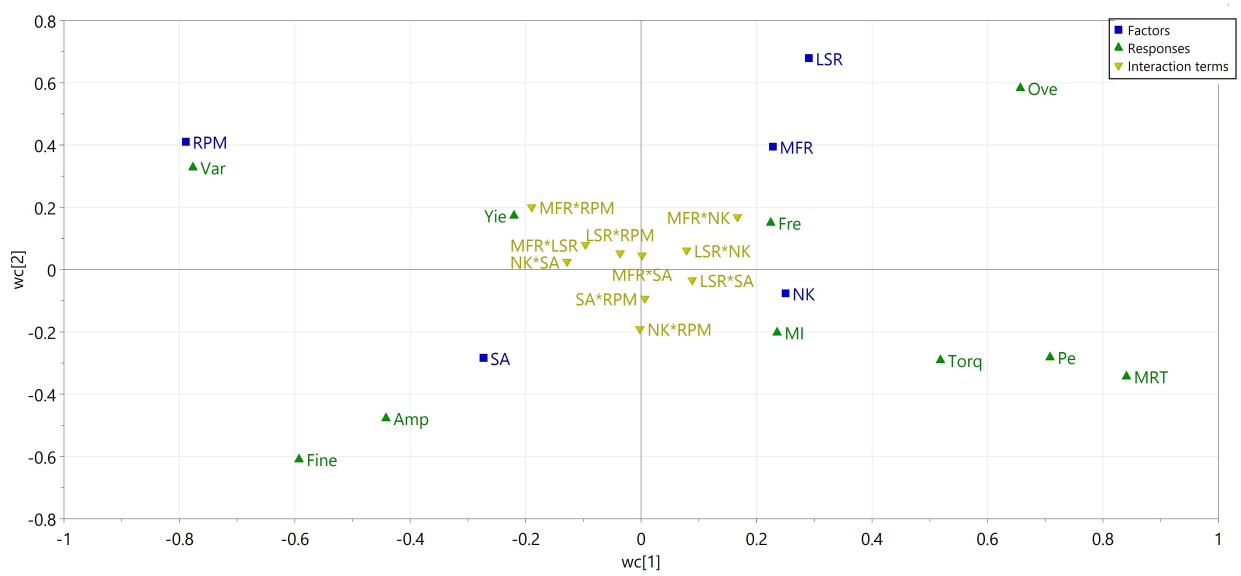

Figure 12: Scatter plot with PLS loadings of the two first model dimensions